

Article

Enhanced Dendrite Resistance in Reversible Electrochemical Pneumatic Batteries with Nanoimprinted Nanowire Anodes for Jamming Robots

Junyu Ge ¹, Yuchen Zhao ¹, Yifan Wang ¹ and Hong Li ^{1,2,3,*} 

¹ School of Mechanical and Aerospace Engineering, Nanyang Technological University, Singapore 639798, Singapore

² School of Electrical and Electronic Engineering, Nanyang Technological University, Singapore 639798, Singapore

³ CNRS-International-NTU-Thales Research Alliance French National Centre for Scientific Research, UMI 3288, Research Techno Plaza, Singapore 637553, Singapore

* Correspondence: ehongli@ntu.edu.sg

Abstract: Traditional electric robots often rely on heavy gear units or expensive force–torque sensors, whereas pneumatic robots offer a cost-effective and simple alternative. However, their dependence on noisy and bulky pneumatic systems, such as compressed air technology, limits their portability and adaptability. To overcome these challenges, we have developed a reversible electrochemical pneumatic battery (REPB) that is compact, noise-free, energy-efficient, and portable. This innovative REPB, principled by the electrochemical redox reactions of zinc–air batteries, can simultaneously supply both electric and pneumatic power, either positive or negative pressure. Its modular, multi-stack structure allows for the easy customization of power output and capacity to suit various applications. We demonstrate the utility of REPB through its application in jamming robots, such as a novel soft yet robust gripper that merges the strengths of hard and soft grippers, enabling universal robotic gripping. This work presents a groundbreaking approach to powering devices that require pneumatic support.



Citation: Ge, J.; Zhao, Y.; Wang, Y.; Li, H. Enhanced Dendrite Resistance in Reversible Electrochemical Pneumatic Batteries with Nanoimprinted Nanowire Anodes for Jamming Robots. *Batteries* **2024**, *10*, 225. <https://doi.org/10.3390/batteries10070225>

Academic Editor: Liubing Dong

Received: 14 May 2024

Revised: 29 May 2024

Accepted: 5 June 2024

Published: 24 June 2024



Copyright: © 2024 by the authors. Licensee MDPI, Basel, Switzerland. This article is an open access article distributed under the terms and conditions of the Creative Commons Attribution (CC BY) license (<https://creativecommons.org/licenses/by/4.0/>).

1. Introduction

Pneumatic-driven components are gaining prominence in robotics due to their impressive power densities, substantial actuating forces, and rapid response times [1–3]. Both pressure and a vacuum are needed for operating various robotic mechanisms [4,5]. However, traditional power sources such as electrical air compressors, compressed gas tanks, and electrical pumps tend to be bulky, rigid, and noisy, which compromises their portability [6,7]. These constraints significantly hinder the development of pneumatic systems, especially in their application to soft autonomous robots [8] and wearable devices [9] that require long-term untethered operation and on-board pressure generation. Consequently, a portable, high-pressure, and quiet-pressure source would be highly beneficial, not only for academic research but also for practical applications in fields like healthcare, search and rescue operations, and exoskeletal technologies.

Various innovative pressure generators have been developed, including electrical dielectric elastomer pumps [10], direct chemical reactions [11,12], and kinds of phase change materials [7], among others. While electrical dielectric elastomer pumps [10] effectively generate gas, their high voltage requirements and limited pressure output restrict their utility for portable applications. Alternative methods like depositing catalysts have been used to enhance on-board gas pressure generation by chemical reaction [8] or direct explosive combustion reaction [13], and yet these techniques pose significant

control and safety challenges. Therefore, there is a substantial demand for a reliable on-board pressure source capable of safely and efficiently generating high pressure, critical for advancing numerous applications.

Metal–air batteries, especially zinc–air batteries (ZABs), are highly valued for their ability to utilize atmospheric oxygen (O_2) as cathode reactants, making them attractive due to their high energy density, abundant materials, low cost, and low toxicity [14–17]. These batteries employ non-toxic aqueous electrolytes with high ionic conductivities, ideal for stationary energy storage due to their stability and high-rate capacities [18]. We have developed an innovative portable reversible electrochemical pneumatic battery based on this kind of ZAB that capitalizes on O_2 to modulate gas generation rates. This rechargeable battery not only supplies electrical power to robotics and sensors but also allows precise control over the volume of gas produced, catering to the specific needs of various robotic applications, a functionality reflected in its name, ‘reversible electrochemical pneumatic battery’.

However, a significant challenge in using zinc as an anode is dendrite growth [19,20], which shortens the battery’s lifespan and reduces the efficiency of electron transfer to oxygen (Faradaic efficiency). Traditional methods to combat dendrite formation, such as using zinc salt with non-aqueous solvents [21] and employing patterned zinc anodes [22], are either costly or impractical at scale. To address this, we propose a novel approach using a room-temperature ultrasonic nanoimprinting method [23] we developed that rapidly patterns rooted nanowires on zinc anodes. These rooted nanowires not only increase the reaction area but also effectively reduce dendrite formation. Our method enables the quick and efficient tuning of a large volume of zinc anodes within minutes, offering a practical solution for enhancing the performance and scalability of zinc–air batteries, further enhancing the REPB performance.

2. Materials and Methods

2.1. Materials

All chemical reagents used in these experiments are of analytical grade and were employed without further purification. All aqueous solutions were prepared using deionized water. The anodic aluminum oxide (AAO) template with 200 nm diameter and 0.1 mm thickness was sourced from Jingyuan Nano Tech., Anhui, China. Potassium hydroxide (KOH) with 85% purity, acetone, 10% platinum/carbon, and ethanol were obtained from Sigma Aldrich, Singapore. Zn foil with 0.1 mm thickness was acquired from High Purity Metal Material Co., Ltd.

2.2. Fabrication of Zn Nanowires

The Zn nanowire anode was fabricated using a cost-effective and scalable ultrasonic nanoimprinting technique recently developed in our group. For more details, please refer to our previously published paper [23]. Prior to the ultrasonic nanoimprinting, zinc (Zn) foils were cut into 1 cm by 1 cm small pieces and then thoroughly cleaned by ultrasonication in acetone, ethanol, and deionized (DI) water, each for a duration of 10 min, to eliminate any impurities. A cleaned Zn piece of 1 cm by 1 cm size was layered with an anodic aluminum oxide (AAO) template of the same size, featuring a pore diameter of 200 nm and thickness of 0.1 mm. This assembly was placed in an ultrasonic nanoimprinting machine with 800 W power (Branson 2000 \times , 20 kHz). The parameters set for fabricating Zn nanowires included an ultrasonic amplitude of 20%, a holding force of 1000 N, and a time duration of 30 s. During the ultrasonic process, a slight noise could be heard due to the vibration. Following the imprinting process, the AAO template, now embedded into the Zn foil, was removed by immersing it in 1 M potassium hydroxide (KOH) for two hours to release the nanowires. Figure 1 illustrates the schematic of the Zn nanowire fabrication process. After that, the prepared Zn nanowire electrode was stored in the Argon atmosphere waiting for the test.

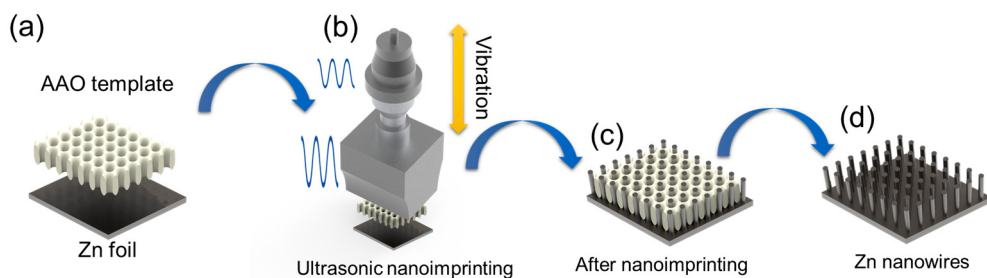


Figure 1. Schematic of Zn nanowire fabrication. (a) Prepared template and Zn foil. (b) Ultrasonic nanoimprinting process. (c) Assembly after nanoimprinting. (d) Fabricated Zn nanowire electrode.

2.3. Reversible Electrochemical Pneumatic Battery

Figure 2 depicts the prototype of the reversible electrochemical pneumatic battery (REPB) that incorporates zinc–air batteries (ZABs) within a sealed unit. The ZAB consists of three components: an air electrode, which is a solid rectangular piece, a Zn anode, and a liquid electrolyte. Therefore, the prototype features a gas chamber with integrated gas ports on a support plate made from polyether ether ketone (PEEK). This design secures the gas electrode and facilitates the collection or consumption of gas in the chamber to create positive pressure or a vacuum. An electrolyte chamber is strategically positioned between the anode and cathode to contain the aqueous KOH solution, ensuring efficient ion transport, and maintaining separation between the electrodes. The zinc anode is sealed on the opposite side by another PEEK plate. The components, electrodes, and electrolytes are securely sealed within the prototype using screws and silicone sealing pads. During the discharge phase, oxygen (O_2) is consumed, creating a vacuum within the gas chamber. Conversely, during the charging phase, O_2 is generated, resulting in high pressure within the chamber. Additionally, the REPB can simultaneously provide electrical power to robotic devices and pneumatic power during discharge.

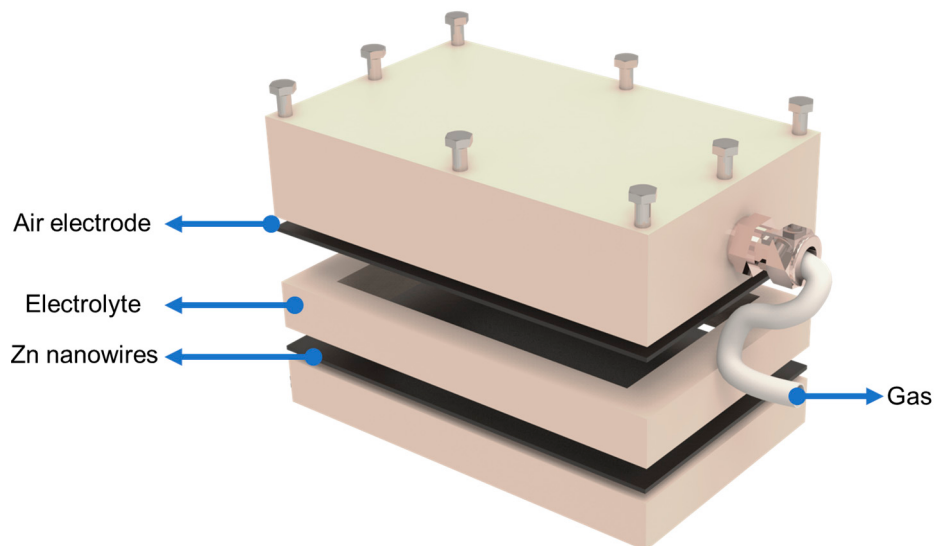


Figure 2. Schematic of prototype designed for reversible electrochemical pneumatic battery.

2.4. Design and Fabrication of Palm-Shape Variable-Stiffness Gripper

The gripper fabrication method is mentioned in our previously published paper [24]. To fabricate the gripper, first, the variable-stiffness materials-based fabric is designed by incorporating structured fabrics known as ‘European 4 in 1’, as shown in Figure 3a, which resemble chain mail and are integrated into the palm part [25]. In the palm part, each fabric piece is intricately woven into four neighboring frames in a consistent pattern. These components are fabricated using a stereolithography 3D printer, specifically the Formlabs

Form3, with clear V4 resin. Each palm assembly includes two pieces of this fabric, which are securely sealed within an air-tight silicone elastomer bag. The silicone bag, made from Smooth-On Ecoflex 30, encases the fabrics in a rectangular shape, ensuring durability and flexibility.

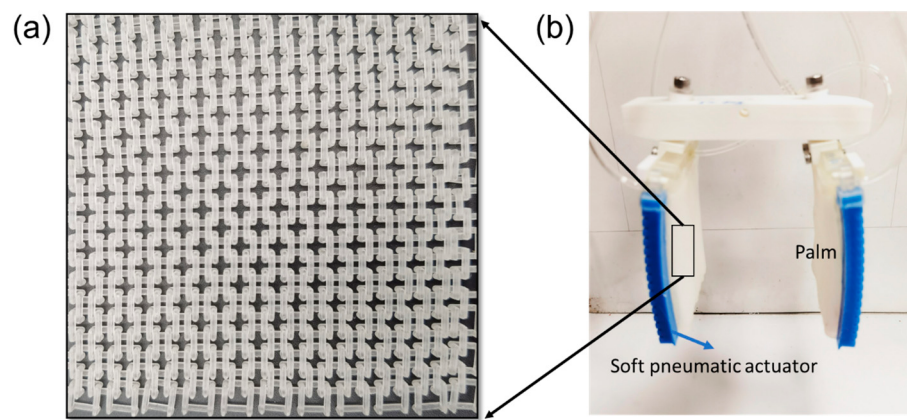


Figure 3. Design and fabrication of gripper's main components. (a) Three-dimensional-printed structured fabrics. (b) Fabricated palm-shaped variable-stiffness gripper.

Additionally, the surface of the silicone bag features a distinctive triangular, zig-zag pattern oriented longitudinally to securely position the fabrics. This zig-zag pattern reduces the palm's bending stiffness, thereby enhancing its conformability when unjammed. A 0.1 mm thin plastic sheet is placed between the fabric and the bag's surface, ensuring full contact in the jammed state and increasing bending stiffness beyond that provided by the silicone membrane alone. Ultimately, the fabric, bag, and plastic sheets are all secured to a rigid connector with an embedded air outlet, forming the structured palm of the gripper as depicted in Figure 3b. This palm requires a vacuum to change states. For detailed insights into the performance and specifications of our design, please refer to our comprehensive paper on the subject [24].

Next, to facilitate the bending of the palm, soft pneumatic actuators are separately fabricated. These actuators require high pressure to bend the variable-stiffness palm and are based on a conventional-fast-pneumatic network design. Each actuator is designed to match the length of the variable-stiffness palm. The body of the actuator is constructed from a silicone elastomer, specifically Smooth-On Mold Star 30.

The variable-stiffness palms and soft pneumatic actuators are linked side-by-side using specialized fixtures and bonding agents. The actuators are meticulously affixed to the central plane of the palm to ensure symmetrical deformation during jamming. Two such palms are vertically aligned and mounted on a horizontal beam to create a parallel jaw configuration typical of industrial grippers. The spacing between the two palms is set at a constant distance.

The system's pneumatic controls are optimized for efficiency through our REPB. Four actuators are connected to the high-pressure output generated by the REPB, with a pressure of 120 kPa being sufficient to induce significant bending of the palms and effectively close the gap between them. Both variable-stiffness palms are also connected to the REPB, which facilitates the generation of a vacuum pump, ensuring synchronized operation across the system.

3. Results and Discussion

3.1. Comparison of Zn Foil and Zn Nanowires

The core element of the reversible electrochemical pneumatic battery is the zinc-air battery. In this battery, zinc is utilized as the anode, while the gas electrode functions as the cathode. The system uses a 6 M potassium hydroxide (KOH) solution as the electrolyte. Figure 4 provides a detailed illustration of the zinc-air battery structure.

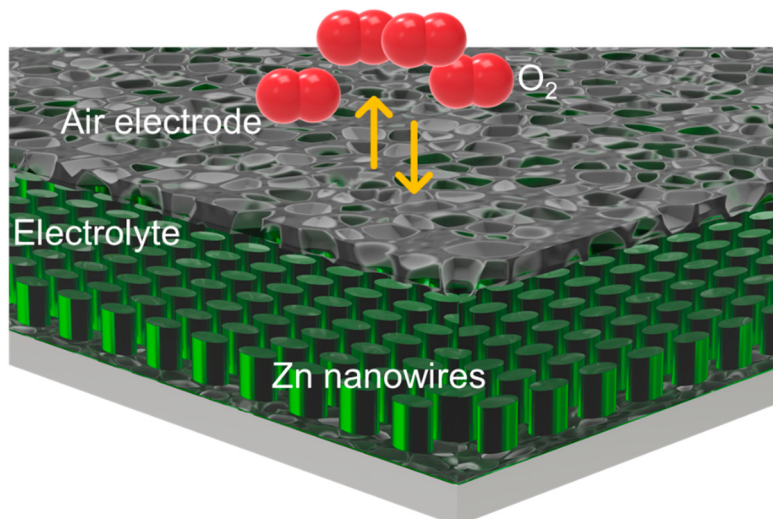
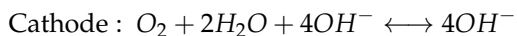
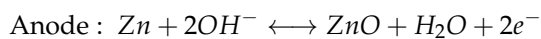


Figure 4. Schematic of zinc–air battery.

The following two consecutive reactions take place at the battery when discharging:



The zinc–air battery operates on a redox reaction between zinc and oxygen in an alkaline electrolyte, specifically producing zinc oxide during discharge. Conversely, during the charging phase, oxygen and zinc are regenerated at the cathode and anode, respectively. This reversible discharge/charge process enables the creation of a vacuum and high-pressure conditions alternately. ZABs are a well-developed technology characterized by their exceptionally high theoretical energy density (1086 Wh/kg) and cost-effectiveness. The entire cycle operates with remarkable efficiency and minimal energy loss. Therefore, although various types of metal–air batteries could serve as the core component of our REPB, we have chosen to use the zinc–air battery for its optimal performance characteristics.

The performance of Zn foil versus Zn nanowires was evaluated through lifespan and durability tests of batteries intended for use in REPB. Due to the high current density requirements of the REPB, both the Zn foil and Zn nanowire anodes were tested at a current density of 100 mA/cm² throughout the entire discharging process. Figure 5 depicts the discharge curves for both setups. Under these conditions, the voltage of the Zn foil anode drops more rapidly, allowing it to operate for only about 120 s. In contrast, the Zn nanowire anode maintains operation for approximately 300 s. This performance indicates that Zn nanowires can sustain larger discharges and store more electrical power than Zn foil, highlighting their superior suitability for applications requiring high current discharges, such as in REPBs.

Subsequent charging and discharging cycling experiments were conducted to assess the endurance of both Zn foil and Zn nanowire anodes (Figure 6). After 150 cycles at a current density of 10 mA/cm², notable differences emerged between the two materials. The operational window of the Zn foil-based battery widened significantly and ceased functioning automatically, while the Zn nanowire-based battery remained relatively stable, with only a slight increase in the charging/discharging voltage window. This indicates a larger increase in resistance in the Zn foil-based zinc–air battery compared to the Zn nanowire-based battery, suggesting better durability and efficiency of the latter in maintaining performance over multiple cycles.

To investigate the observed increase in resistance, we examined the surface morphology changes of both the Zn foil and Zn nanowire anodes using scanning electron microscopy (SEM), as depicted in Figure 7. The SEM images revealed a marked contrast in dendritic

growth between the two samples. The Zn foil showed large, randomly formed porous dendrites, whereas dendritic growth on the Zn nanowires was significantly mitigated. This reduction in dendritic growth on the nanowires is attributed to the dendrites growing along the nanowire diameter direction, as illustrated in Figure 7d. Such confined growth restricts the dendritic coverage to just the surface of the nanowires, resulting in a total dendrite thickness of only a few micrometers. In contrast, dendrites on the Zn foil can reach hundreds of micrometers in thickness, and the porous structure significantly increases the resistance of the Zn anode. Thus, our ultrasonic nanoimprinting-based approach for creating Zn nanowires effectively inhibits dendrite growth and enhances battery performance.

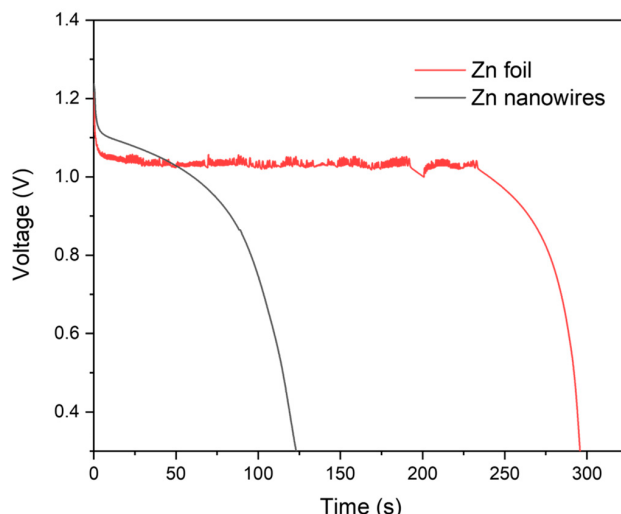


Figure 5. Discharge measurements of Zn foil and Zn nanowires.

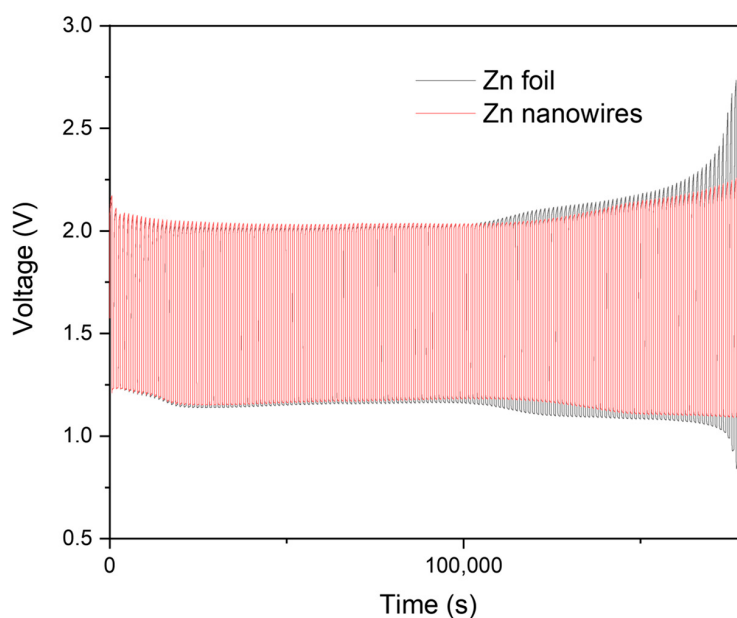


Figure 6. Cycling measurements of Zn foil and Zn nanowires.

To further demonstrate the inhibition of Zn dendrite growth, we have included X-ray Photoelectron Spectroscopy (XPS) results of O1s peaks. Compared with Zn nanowires, the dendrites on the Zn foil exhibit a significant peak related to $\text{Zn}(\text{OH})_2$, which is negligible in the Zn nanowire sample. $\text{Zn}(\text{OH})_2$ is more soluble and variable in humid environments, while ZnO is relatively more stable. A high proportion of $\text{Zn}(\text{OH})_2$ suggests that the dendrites are less stable in the electrolyte, making them prone to morphological changes or detachment, which can adversely affect the battery's cycling performance and lifespan.

The ratio of ZnO to Zn(OH)₂ can also indicate the electrochemical reactions occurring within the battery. For instance, a higher proportion of Zn(OH)₂ might indicate more side reactions during charging, consuming zinc and leading to rapid dendrite growth. The formation of Zn(OH)₂ and ZnO is related to the corrosion behavior of zinc in the electrolyte. The presence of Zn(OH)₂ usually indicates higher corrosion activity on the electrode surface, while ZnO might be a product of corrosion that offers some protection.

Therefore, compared to the Zn foil, which has a large ratio of Zn(OH)₂, the Zn nanowire sample demonstrates better performance. The related results are shown in Figure 8.

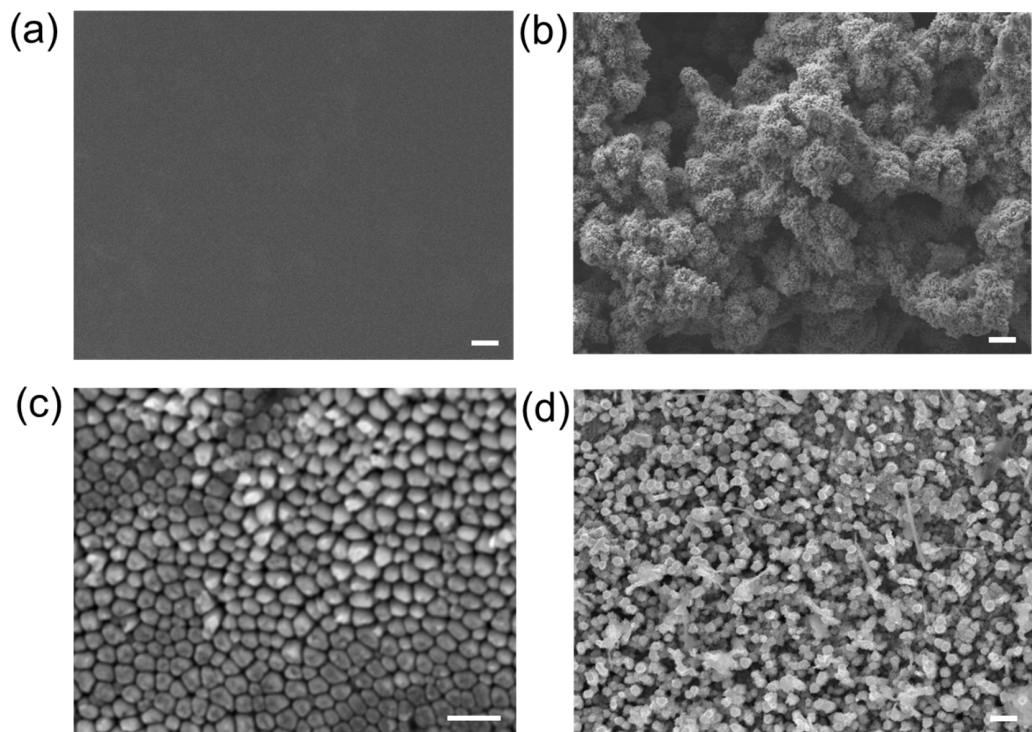


Figure 7. SEM images of Zn foil and Zn nanowires before and after reaction. (a,b) Zn foil before and after cycling measurements. Scale bars of (a,b) are 10 μm . (c,d) Zn nanowires before and after cycling measurements. Scale bars of (c,d) are 1 μm .

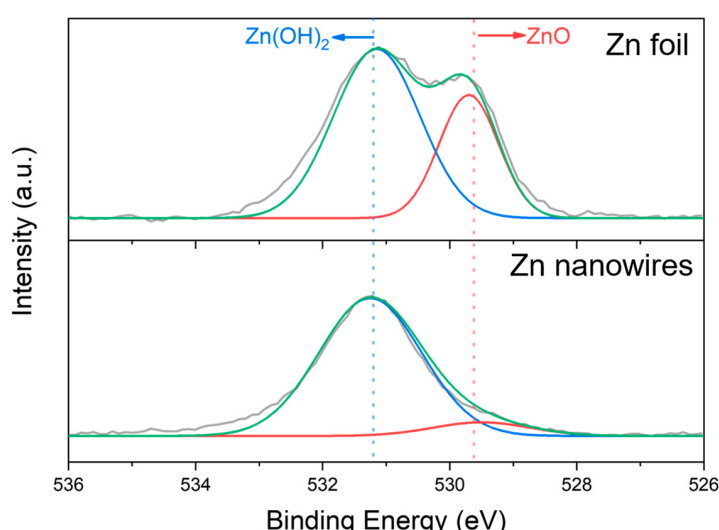


Figure 8. XPS spectra of O1s region for Zn foil and Zn nanowire samples after reaction. In this figure, the red line represents the peak related to ZnO, the blue line represents the peak related to Zn(OH)₂, the green line is the fitted result, and the grey line is the measured result.

What is more, linear sweep voltammetry (LSV) results supported the conclusion as well, as shown in Figure 9. After 150 cycles, the discharging process LSV of Zn nanowires remains over 300 mA/cm² in a single LSV scanning, whereas the Zn foil exhibits less than 200 mA/cm². The current density of Zn nanowires is almost twice that of Zn foil. This indicates that, compared to Zn nanowires, the Zn foil shows worse performance with higher resistance and lower activation, resulting in a significantly lower current.

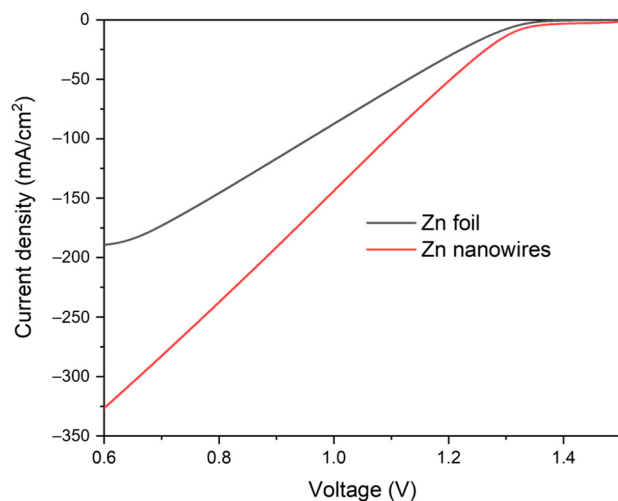


Figure 9. The LSV spectra of the Zn foil and Zn nanowire samples after 150 cycles.

3.2. Pressure Generation Ability Measurements

An accurate regulation of the pressure generation process in REPB systems necessitates high efficiency in gas generation, quantified by the Faradaic efficiency (FE). Faradaic efficiency measures how effectively the electric charge from the power supply is used to produce or consume oxygen. It is estimated by comparing the charge required for the measured volume of oxygen (Q_{oxygen}) to the total charge transferred from the power supply to the battery (Q_{supply}). The latter is calculated by multiplying the constant current (i) by the charging duration (t). A 100% FE indicates that all electrons from the power supply are utilized for oxygen production without any by-products or side reactions. The FE can be calculated using the following equation:

$$\text{Faradaic efficiency} = \frac{Q_{\text{oxygen}}}{Q_{\text{supply}}} \times 100\% = \frac{z \times n \times F}{i \times t} \times 100\%$$

where

- $z = 4$ is the number of electrons involved in generating one molecule of O₂,
- n is the number of moles of O₂ generated,
- $F = 96,000$ C/mol is the Faraday constant,
- i is the charging current,
- t is the charging duration.

After carefully calculating the generated gas volume and the electrical power used, we confirm that the Faradaic efficiency of our REPB exceeds 95%. This high FE underscores the efficient gas generation capabilities of our REPB, demonstrating its effectiveness in utilizing electrical power to produce gas with minimal energy loss.

Different applications may require varying amounts of gas. For instance, transporting large or heavy objects with a large gripper necessitates a significant volume of gas. To address this need, it is crucial to effectively scale up the generated pressure for varying gas volumes with our REPB. To demonstrate this scaling capability, we fabricated a battery with a reaction area of 150 cm² and measured the pressure changes over time, as depicted in Figure 10. With a contained volume of 20 mL, the pressure can decrease from 0 bar

(standard atmospheric pressure) to -0.6 bar in less than 2 min when discharging at 3 A, and it can increase from 0 bar to 1.75 bar in under two minutes when charged at 5 A.

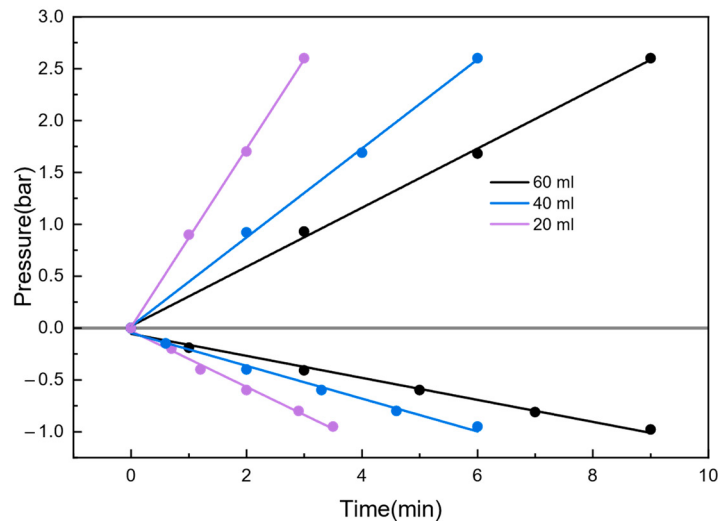


Figure 10. Relationship between pressure and time under different gas volumes.

For a larger required gas volume set at 60 mL, approximately the total volume when the battery is connected to a palm-shaped variable-stiffness gripper, the pressure changes more gradually. It drops to -0.6 bar or rises to 1.25 bar over a span of 5 min during discharging or charging, respectively. The pressure change over time remains linear for constant current operations across various volumes. The Faradaic efficiency (FE) at different volumes is nearly 100%, indicating that the battery maintains exceptional performance even when scaled up. For needs involving less than 20 mL, this reaction area enables rapid operations under high pressure or in a vacuum. Moreover, if faster operations or higher gas volumes are required, the number of batteries can be simply increased. Consequently, the EPB demonstrated in this study is highly scalable and can be adapted to suit a broad range of applications.

3.3. Reversible Electrochemical Pneumatic Battery Connection to Gripper

We demonstrate the utility of our REPB as a quiet, efficient source of both high pressure and a vacuum for the palm-shaped variable-stiffness gripper based on 3D-printed fabric jamming, as highlighted in Figure 11. The details of this gripper are shown in our previous paper [24]. Briefly, this gripper achieves a maximum gripping force of 17 N. Due to the discrete nature of the fabrics, our gripper conforms well to varied shapes, enhancing its utility. This gripping conformability has been quantitatively characterized in the paper. The superior gripping-to-pinch force ratio and outstanding conformability of the design exceed those of conventional universal grippers and jamming-based anthropomorphic soft grippers. The former typically necessitates considerable pushing force, whereas the latter, although adept at managing delicate objects, often falls short in terms of conformability and rigidity. Moreover, the design is well-suited for handling fragile items and marks a step toward utilizing robotic surfaces for gripping tasks, promising broad applications in sectors like packaging, logistics, food, and agriculture.

Here, the REPB cell's gas outlet is connected to the gripper via tubing and valves, ensuring an airtight system. Initially, the REPB is charged by connecting its electrodes to an electrical power source. During this process, the gas chamber is linked to soft pneumatic actuators (the blue parts), and the generated positive pressure in the gas chamber bends the soft pneumatic grippers. This action also causes the variable-stiffness palm to bend appropriately, enabling it to grasp objects effectively. Subsequently, the REPB is connected to a variable-stiffness palm (the white parts) by adjusting the valve. It then discharges through a load to consume the oxygen inside the gas chamber, creating a vacuum that

significantly increases the palm's stiffness, enabling it to securely grasp objects. Figure 11b depicts the gripper grasping an object. The entire operation is motor-free, thus remaining exceptionally quiet. Although the REPB cell appears large, this is primarily because of the hard metal spacer needed to generate pressures above 10 bar for universal applications. However, in this scenario, only 120 kPa of positive pressure is necessary, allowing for a significant reduction in size if necessary.

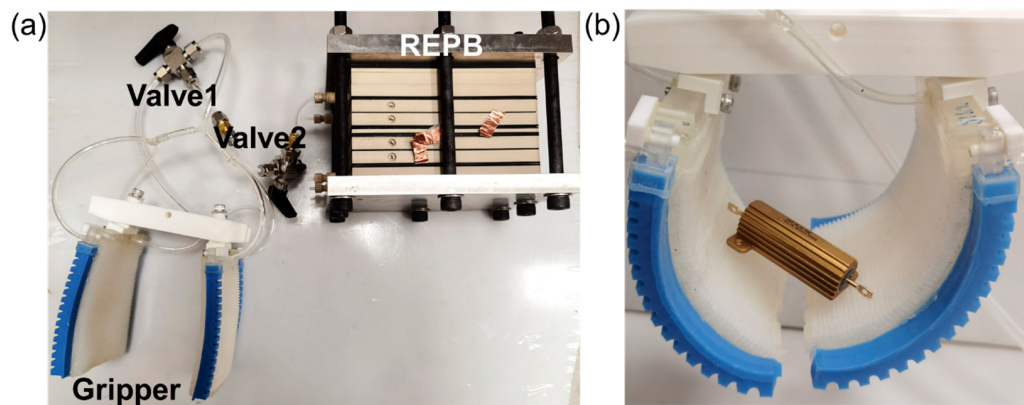


Figure 11. The REPB connected to a palm-shaped variable stiffness gripper. (a) The gas connection system between the REPB and the gripper. (b) The gripper grasping an object.

4. Conclusions

In this paper, an innovative REPB is introduced that directly converts electrical energy into pneumatic pressure via a redox electrochemical reaction related to a zinc–air battery. Characterized by its compact structure, energy conservation, and silent functionality, this battery offers a distinct alternative to conventional motor-driven pumps. Its electrodes are easily trimmable sheet structures, which not only facilitate easier production but also enhance mechanical versatility and the potential for scaling. Unlike pressure generation methods based on irreversible or extreme chemical reactions such as explosions, the REPB is reversible and allows for precise pressure control through adjustments to the electric current. It also boasts enhanced safety compared to regenerative fuel cells which generate a mixture of hydrogen and oxygen, as it exclusively uses oxygen as the working gas. More importantly, the use of a nanowire Zn anode significantly enhances the oxygen uptake capability, durability, and cycle robustness of the pneumatic battery, thereby greatly improving the performance of the REPB. Additionally, our Zn nanowire fabrication method employs a rapid ultrasonic technique that can complete nanoimprinting within minutes. This method facilitates the easy production of large-scale nanowire-based electrodes and is energy-efficient. The demonstration shows that the REPB can serve as a replacement for traditional air electrical pumps in applications requiring both positive pressure and vacuum, such as a palm-shaped variable-stiffness gripper. Although our demonstrations are currently on the centimeter scale and our fabrication process is limited to manual operation, the proposed pneumatic battery can be fabricated on a larger scale, and the fabrication process can be automated. The lifespan of the REPB is currently mediocre compared to other batteries like lithium-ion batteries, due to the sluggish development of metal–air rechargeable battery technology. However, we believe that with further advancements in metal–air rechargeable battery technology, the lifespan of the REPB will improve significantly. The concept of a reversible electrochemical pneumatic battery, along with the use of Zn nanowire-based electrodes in this work, is expected to significantly influence the development of new pneumatic sources.

5. Patent

H.L. is an inventor on a patent application related to this work, filed by Nanyang Technological University Singapore (Application no.: 202180011805.4 and 11202252422A).

J.G. and H.L. are inventors on a patent application related to this work, filed by Nanyang Technological University Singapore (publication no. WO 2022/045965 A1).

Author Contributions: Conceptualization, H.L.; methodology, J.G. and Y.Z.; validation, J.G.; investigation, J.G.; resources, J.G. and Y.Z.; data curation, J.G. and Y.Z.; writing—original draft preparation, J.G.; supervision, H.L. and Y.W. All authors have read and agreed to the published version of the manuscript.

Funding: This work was supported by the A*STAR Science and Engineering Research Council MTC IRG funding (M21K2c0118), the Ministry of Education Singapore (Award No: MOE-T2EP50221-0002), and the Ministry of Education Singapore (Award No: MOE-T2EP50123-0016).

Data Availability Statement: Data is contained within the article.

Conflicts of Interest: The authors declare no conflict of interest.

References

- Chauhan, M.; Chandler, J.H.; Jha, A.; Subramaniam, V.; Obstein, K.L.; Valdastri, P. An Origami-Based Soft Robotic Actuator for Upper Gastrointestinal Endoscopic Applications. *Front. Robot. AI* **2021**, *8*, 664720. (In English) [[CrossRef](#)]
- Zhang, J.; Sheng, J.; O'Neill, C.T.; Walsh, C.J.; Wood, R.J.; Ryu, J.-H.; Desai, J.P.; Yip, M.C. Robotic Artificial Muscles: Current Progress and Future Perspectives. *IEEE Trans. Robot.* **2019**, *35*, 761–781. [[CrossRef](#)]
- Wolbrecht, E.T.; Reinkensmeyer, D.J.; Bobrow, J.E. Pneumatic Control of Robots for Rehabilitation. *Int. J. Robot. Res.* **2009**, *29*, 23–38. [[CrossRef](#)]
- Papadakis, E.; Raptopoulos, F.; Koskinopoulou, M.; Maniadakis, M. On the Use of Vacuum Technology for Applied Robotic Systems. In Proceedings of the 2020 6th International Conference on Mechatronics and Robotics Engineering (ICMRE), Barcelona, Spain, 12–15 February 2020; pp. 73–77. [[CrossRef](#)]
- Adami, M.; Seibel, A. On-Board Pneumatic Pressure Generation Methods for Soft Robotics Applications. *Actuators* **2019**, *8*, 2. [[CrossRef](#)]
- Cacucciolo, V.; Shintake, J.; Kuwajima, Y.; Maeda, S.; Floreano, D.; Shea, H. Stretchable pumps for soft machines. *Nature* **2019**, *572*, 516–519. [[CrossRef](#)]
- Wehner, M.; Tolley, M.T.; Mengüç, Y.; Park, Y.-L.; Mozeika, A.; Ding, Y.; Onal, C.; Shepherd, R.F.; Whitesides, G.M.; Wood, R.J. Pneumatic energy sources for autonomous and wearable soft robotics. *Soft Robot.* **2014**, *1*, 263–274. [[CrossRef](#)]
- Wehner, M.; Truby, R.L.; Fitzgerald, D.J.; Mosadegh, B.; Whitesides, G.M.; Lewis, J.A.; Wood, R.J. An integrated design and fabrication strategy for entirely soft, autonomous robots. *Nature* **2016**, *536*, 451–455. [[CrossRef](#)] [[PubMed](#)]
- Park, Y.-L.; Santos, J.; Galloway, K.G.; Goldfield, E.C.; Wood, R.J. A soft wearable robotic device for active knee motions using flat pneumatic artificial muscles. In Proceedings of the 2014 IEEE International Conference on Robotics and Automation (ICRA), Hong Kong, China, 31 May–7 June 2014; IEEE: Piscataway, NJ, USA; pp. 4805–4810.
- Cao, C.; Gao, X.; Conn, A.T. A magnetically coupled dielectric elastomer pump for soft robotics. *Adv. Mater. Technol.* **2019**, *4*, 1900128. [[CrossRef](#)]
- Okui, M.; Nagura, Y.; Iikawa, S.; Yamada, Y.; Nakamura, T. A pneumatic power source using a sodium bicarbonate and citric acid reaction with pressure booster for use in mobile devices. In Proceedings of the 2017 IEEE/RSJ International Conference on Intelligent Robots and Systems (IROS), Vancouver, BC, Canada, 24–28 September 2017; IEEE: Piscataway, NJ, USA; pp. 1040–1045.
- Shields, B.L.; Fite, K.B.; Goldfarb, M. Design, control, and energetic characterization of a solenoid-injected monopropellant-powered actuator. *IEEE/ASME Trans. Mechatron.* **2006**, *11*, 477–487. [[CrossRef](#)]
- Shepherd, R.F.; Stokes, A.A.; Freake, J.; Barber, J.; Snyder, P.W.; Mazzeo, A.D.; Cademartiri, L.; Morin, S.A.; Whitesides, G.M. Using explosions to power a soft robot. *Angew. Chem. Int. Ed.* **2013**, *52*, 2892–2896. [[CrossRef](#)]
- Park, J.; Park, M.; Nam, G.; Lee, J.; Cho, J. All-solid-state cable-type flexible zinc-air battery. *Adv. Mater.* **2014**, *27*, 1396–1401. [[CrossRef](#)] [[PubMed](#)]
- Liu, X.; Yuan, Y.; Liu, J.; Liu, B.; Chen, X.; Ding, J.; Han, X.; Deng, Y.; Zhong, C.; Hu, W. Utilizing solar energy to improve the oxygen evolution reaction kinetics in zinc–air battery. *Nat. Commun.* **2019**, *10*, 4767. [[CrossRef](#)] [[PubMed](#)]
- Fu, J.; Lee, D.U.; Hassan, F.M.; Yang, L.; Bai, Z.; Park, M.G.; Chen, Z. Flexible high-energy polymer-electrolyte-based rechargeable zinc–air batteries. *Adv. Mater.* **2015**, *27*, 5617–5622. [[CrossRef](#)] [[PubMed](#)]
- Mainar, A.R.; Colmenares, L.C.; Grande, H.-J.; Blázquez, J.A. Enhancing the cycle life of a zinc–air battery by means of electrolyte additives and zinc surface protection. *Batteries* **2018**, *4*, 46. [[CrossRef](#)]
- Wang, F.; Borodin, O.; Gao, T.; Fan, X.; Sun, W.; Han, F.; Faraone, A.; A Dura, J.; Xu, K.; Wang, C. Highly reversible zinc metal anode for aqueous batteries. *Nat. Mater.* **2018**, *17*, 543–549. [[CrossRef](#)] [[PubMed](#)]
- Stock, D.; Dongmo, S.; Janek, J.R.; Schro, D. Benchmarking anode concepts: The future of electrically rechargeable zinc–air batteries. *ACS Energy Lett.* **2019**, *4*, 1287–1300. [[CrossRef](#)]
- Li, Y.; Dai, H. Recent advances in zinc–air batteries. *Chem. Soc. Rev.* **2014**, *43*, 5257–5275. [[CrossRef](#)] [[PubMed](#)]

21. Pan, Z.; Yang, J.; Zang, W.; Kou, Z.; Wang, C.; Ding, X.; Guan, C.; Xiong, T.; Chen, H.; Zhang, Q.; et al. All-solid-state sponge-like squeezable zinc-air battery. *Energy Storage Mater.* **2019**, *23*, 375–382. [[CrossRef](#)]
22. Shinde, S.S.; Jung, J.Y.; Wagh, N.K.; Lee, C.H.; Kim, D.-H.; Kim, S.-H.; Lee, S.U.; Lee, J.-H. Ampere-hour-scale zinc-air pouch cells. *Nat. Energy* **2021**, *6*, 592–604. [[CrossRef](#)]
23. Ge, J.; Ding, B.; Hou, S.; Luo, M.; Nam, D.; Duan, H.; Gao, H.; Lam, Y.C.; Li, H. Rapid fabrication of complex nanostructures using room-temperature ultrasonic nanoimprinting. *Nat. Commun.* **2021**, *12*, 3146. [[CrossRef](#)]
24. Zhao, Y.; Wang, Y. A Palm-Shape Variable-Stiffness Gripper Based on 3D-Printed Fabric Jamming. *IEEE Robot. Autom. Lett.* **2023**, *8*, 3238–3245. [[CrossRef](#)]
25. Wang, Y.; Li, L.; Hofmann, D.; Andrade, J.E.; Daraio, C. Structured fabrics with tunable mechanical properties. *Nature* **2021**, *596*, 238–243. [[CrossRef](#)] [[PubMed](#)]

Disclaimer/Publisher’s Note: The statements, opinions and data contained in all publications are solely those of the individual author(s) and contributor(s) and not of MDPI and/or the editor(s). MDPI and/or the editor(s) disclaim responsibility for any injury to people or property resulting from any ideas, methods, instructions or products referred to in the content.